

## Modelling of wave damping at Guyana mud coast

J.C. Winterwerp<sup>a,b,\*</sup>, R.F. de Graaff<sup>a</sup>, J. Groeneweg<sup>a</sup>, A.P. Lujendijk<sup>a</sup>

<sup>a</sup> Delft Hydraulics, PO Box 177, 2600 MH Delft, The Netherlands

<sup>b</sup> Delft University of Technology, Delft, The Netherlands

Received 23 November 2005; received in revised form 17 July 2006; accepted 30 August 2006

Available online 20 October 2006

### Abstract

The Guyana coastal system is characterized by very thick deposits of Amazon mud and high mud concentrations in its coastal waters. The mud deposits can be quite soft and may liquefy under incoming waves. Subsequently, the liquefied mud damps the incoming waves effectively. This paper presents a simple model to predict wave attenuation over soft (fluid) mud beds. This model is based on the two-layer approach by Gade [Gade, H.G., 1958, Effects of a non-rigid, impermeable bottom on plane surface waves in shallow water, *Journal of Marine Research*, 16 (2) 61–82.] which is implemented in the standard version of the state-of-the-art wave-prediction model SWAN. Input to the mud wave damping module consists of the extension, thickness, density and viscosity of the liquefied (fluid) mud layer.

The model is validated against small-scale wave attenuation measurements carried out in a laboratory wave flume. The model predictions agree favourably with the experimental data. Next, the model is applied to predict wave height and wave attenuation in the Guyana coastal system. Extension and thickness of the liquefiable layer could be assessed from dual-frequency echo soundings. In the absence of field data, the density of the liquefied mud layer is obtained from literature, whereas the value of the mud's viscosity had to be established by trial and error — the selected value, though, is in the range of literature values. The model predicts significant wave attenuation. The computed changes in wave energy spectrum agree qualitatively with measurements in Surinam, whereas the decrease in significant wave height agrees more or less with historic observations along the Guyana coast.

© 2006 Elsevier B.V. All rights reserved.

*Keywords:* Guyana mud coast; Fluid mud; Wave damping; SWAN

### 1. Introduction

The Guiana coastal system, stretching from the Amazon to the Orinoco River is very muddy with mud deposits of many 100 m thickness, with extreme values of about 1800 m near New Amsterdam (NEDECO, 1972). The major part of this mud has originated from the Amazon catchment area; sediment input from local rivers is small (e.g. Fig. 1, Augustinus, 1978). The sediment is carried by the Amazon coastal plume, which is maintained within a narrow band of a few 10 km width along the coast by the Trade Winds and by the conservation of potential vorticity, preventing the plume to drift towards deeper water. The accompanying cross-shore salinity gradients generate a cross-shore gravitational circulation, which also keeps the sediment

near the coast. As such, the entire Guiana coastal system forms part of the greater Amazon delta.

Along the entire coast from the Amazon to the Orinoco River, wide fringes of mangrove forests are found. This mud–mangrove coastal system is highly dynamic, characterized by large natural erosion and accretion rates, which are related to, amongst other things, the migration of huge mud banks along the coast at a periodicity of about 30 years (Wells and Coleman, 1981; Allison and Lee, 2004). However, along large stretches of the coast of British Guyana, the natural accretion processes are disturbed, resulting in serious erosion of the coast. Where this is the case, hard sea defences are required to protect the hinterland from flooding. One of the boundary conditions for the design of such sea defences consists of the local expected wave height.

It has been shown that waves can be damped by soft mud layers (e.g. Gade, 1958; Kurup, 1972), as observed in the Guyana coastal system. Tubman and Suhayda (1976) carried out measurements in 1976 in the East Bay near the Mississippi

\* Corresponding author. Delft Hydraulics, PO Box 177, 2600 MH Delft, The Netherlands.

E-mail address: [han.winterwerp@wldelft.nl](mailto:han.winterwerp@wldelft.nl) (J.C. Winterwerp).

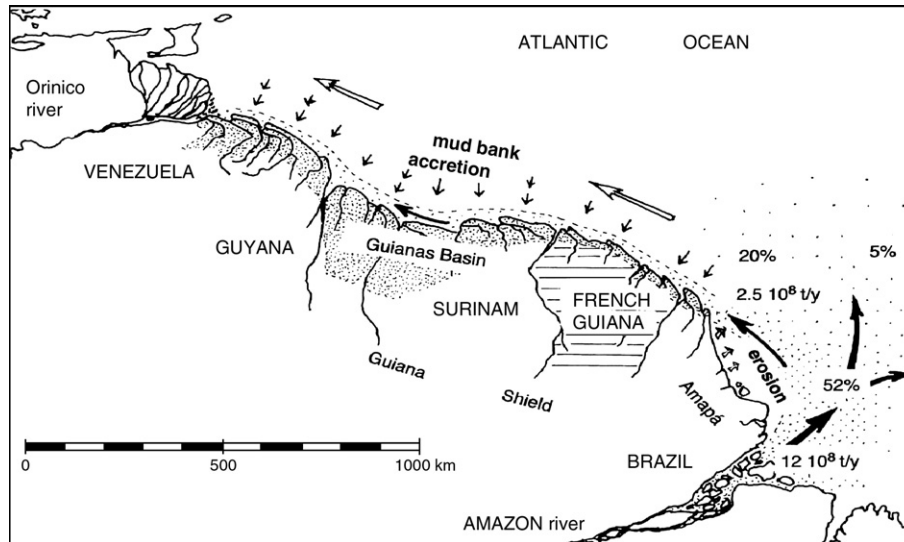


Fig. 1. Sketch of sediment fluxes in Guiana coastal system (after Augustinus, 1978).

mouth at two stations at 20 and 3.5 m water depth and 3.5 km apart. The bed consists of thick layers (several 10 m) of soft mud with a strength close to the liquid limit (1.75–2.36 kPa). From a simple estimation on the wave damping to be expected solely by bed friction, they concluded that the wave height was dissipated within the soft mud by about 50% over this 3.5 km trajectory.

Recently, Sheremet and Stone (2003) analyzed wave measurements over five days in early 2001 at two stations located at the 5 m isobath offshore Atchafalaya Bay. One station was located above a sandy seabed, and the other over a muddy seabed. Though these stations were 150 km apart, the incoming wave conditions and local wind climate were so similar that a comparison of wave heights at these stations was considered meaningful. They observed significantly lower wave heights (more than 70% smaller) at the muddy site in comparison with the sandy site. This damping was attributed to dissipation of wave energy in the mud layers. Moreover, they observed wave damping throughout the entire energy spectrum, which was unexpected as one would expect that the shorter waves would not be affected by the muddy seabed.

Wells and Kemp (1986) measured wave heights in the coastal area of Surinam at three stations at 7.1, 4.7 and 3.1 m water depth approximately 21.1, 11.7 and 4.3 km off the coast, respectively. This coastal area is characterized by thick layers of Amazon mud (thickness exceeding a few 100 m). They observed 88% and 96% dissipation of the wave energy traveling from the most seaward monitoring station towards the shore (see Fig. 5). It is noted that also in this case dissipation over the entire energy spectrum was observed, though the longer waves dissipated the most.

Conceptually, wave damping over muddy beds is characterized by a sequence of events. First, small elastic deformations are generated within the seabed by the cyclical stresses induced by the incoming waves. At the moment these stresses exceed the strength of the bed, internal failure occurs resulting in the liquefaction of (part of) the seabed. This is a fairly rapid process, i.e. of the order of tens of seconds, up to a few minutes at most, e.g. Foda

and Tzang (1994), Lindenberg et al. (1989), De Wit (1995), De Wit and Kranenburg (1997). The bed can then be characterized as fluid mud. The incoming waves now generate internal waves at the mud–water interface, which are dissipated by internal friction within the fluid mud layer. More sediment may liquefy below this fluid mud layer, but this is not likely because:

- the fluid mud layer damps the waves, hence the stresses within the bed,
- earlier events (stress history) tend to limit the thickness of the bed that is sensitive to liquefaction.

Hence, one may conclude that the (maximum) thickness of the liquefiable bed is a characteristic feature of a specific coastal system. This thickness is determined by the mud properties and the wave climate, which together also determine the important stress history. Moreover, erosion of the mud layer may occur and must be accounted for, though over a somewhat larger time scale.

The first modelling study known to the authors on wave attenuation over muddy beds was carried out by Gade (1958), who treated the water–bed system as a two-layer fluid system, in

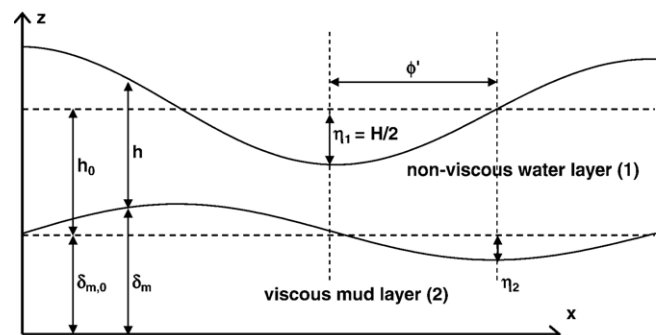


Fig. 2. Sketch of two-layer fluid mud system and definitions (after Gade, 1958).

which the upper layer consists of (non-viscous) water, and the lower layer a highly viscous fluid mud. Details of Gade’s model are further discussed later in this paper.

Many authors have noted that Gade’s two-layer model cannot be complete, because it ignores the effects of viscosity in the upper layer, as well as the effects of elasticity, porosity and plasticity in the lower layer, as discussed above. As a result, several other models have been proposed since Gade’s pioneering work. Dalrymple and Liu (1978) and Jiang and Zhao (1989) extended Gade’s model by including viscosity in the upper layer. Golden et al. (1982) argued that water–mud mixtures at concentrations typical of fluid mud reveal important elastic properties, and many authors have proposed visco-elastic models to describe the behaviour of fluid mud and the subsequent wave damping. The viscous and elastic components of such models can be coupled in a series (Kelvin–Voigt model, e.g. MacPherson, 1980; Chou et al., 1993) or in parallel (Maxwell model, e.g. Maa, 1986; Maa and Mehta, 1990; Rodriguez, 2000; Rodriguez and Mehta, 2001). Jiang (1993) and Mehta (1996) even proposed to combine the serial and parallel coupling through a three-element approach.

Another series of models was proposed by Mei and Liu (1987) and Liu and Mei (1989) in which the effects of plastic deformations of the muddy seabed are accounted for in a so-called visco-plastic approach. The well-known Bingham model is one of the simplest visco-plastic models used, but a number of other models have also been elaborated, such as the general-plastic Herschel–Bulkley model. Liu (1973), Yamamoto et al. (1978), Yamamoto and Takahashi (1985) and Spierenburg (1987) included the effects of porosity of the seabed through a poro-elastic description. Verbeek and Cornelisse (1997) applied a poro-elasto-viscous model.

Some of the proposed models are quite simple, but others are so complicated that computational times become prohibitively large when implemented in an engineering environment. Moreover, none of the models cover the entire range of conditions encountered under natural conditions. Chou (1989, 1993), for instance, shows that the shear and loss moduli of visco-elastic models may vary with the frequency of the externally applied stresses, reducing the validity of such models. Furthermore, it can be reasoned that elastic effects are small anyway when the muddy seabed is liquefied, and do not yield energy losses, hence do not contribute to wave damping. However, changes in elasticity

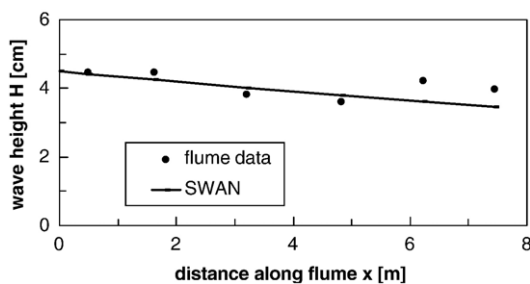


Fig. 3. Comparison of measured and computed wave heights in laboratory flume.

Table 1  
Mud parameters in SWAN mud wave damping model (after De Wit, 1995)

$\rho_w$ [kg/m <sup>3</sup> ]	$\rho_m$ [kg/m <sup>3</sup> ]	$\delta_{m,0}$ [m]	$h_0$ [m]	$H_0$ [m]	$\nu_m$ [m <sup>2</sup> /s]	$\alpha$
1000	1300	0.115	0.325	0.045	$2.6 \cdot 10^{-3}$	1

do change the viscosity of the mud, hence affect the possible flow of the mud. Winterwerp and Van Kesteren (2004) show that the response of muddy deposits to external forces is basically governed by undrained processes as the permeability of the mud is very small, hence the relevant Peclet number becomes quite large. As porous effects also do not contribute to energy losses in the mud, we can ignore these porous effects to first order.

As argued above, energy losses are to be expected by plastic deformation, liquefying the muddy seabed. However, as also said, liquefaction is a rapid process, and therefore plastic losses occur during a limited time only, i.e. much smaller than stormy periods in general.

Hence, in our model we propose to account for viscous damping of incoming waves only. We elaborate on Gade’s model and implement his two-layer model, though slightly modified, in the standard SWAN-code, as described in Section 2. SWAN is a third generation wave-prediction model that is freely available. The modified model is validated against laboratory measurements in Section 3 and applied to the Guyana coastal system in Section 4. In the next phase of our study, we will include wave-induced fluid mud transport in a two-layer schematisation of the water–fluid mud system, the lower fluid mud layer being depth-averaged.

## 2. Modelling of fluid mud-induced viscous wave damping

The two-layer fluid mud model by Gade (1958) is modified slightly and implemented in the SWAN wave model. The SWAN model is a two-dimensional fully spectral state-of-the-

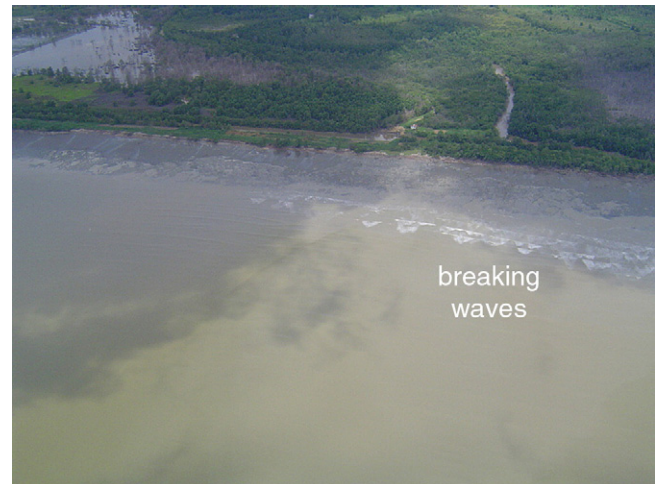


Fig. 4. Aerial photograph of wave braking and wave damping at the Demerara coast, Guyana.

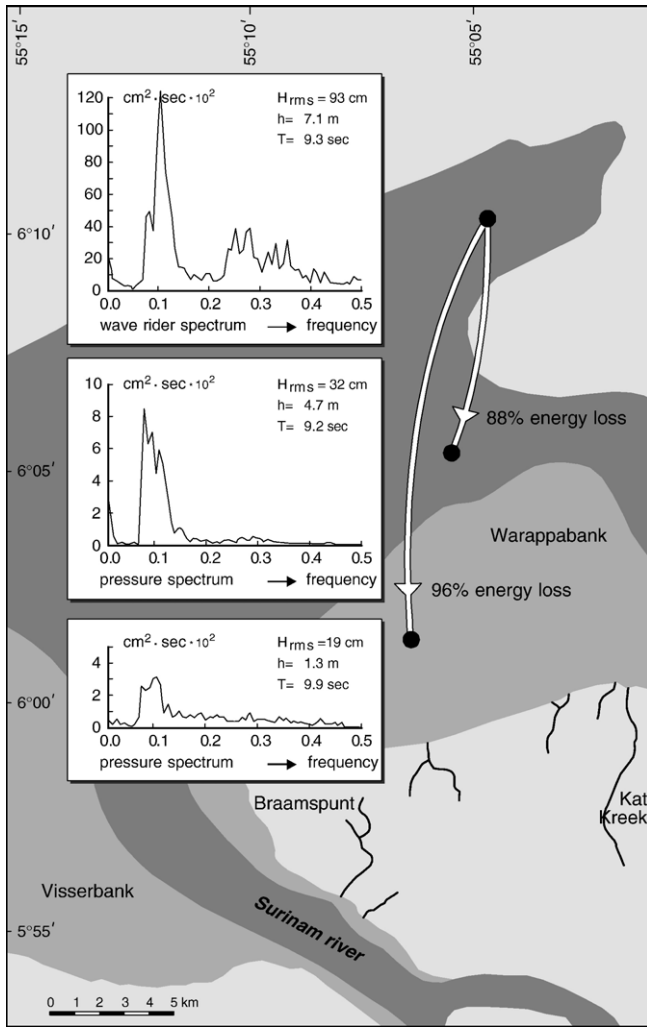


Fig. 5. Wave attenuation measured in Surinam coastal system (after Wells and Kemp, 1986).

art wave propagation model developed by Delft University of Technology (Booij et al., 1999; Zijlema and van der Westhuijsen, 2005). SWAN solves the balance equation for

wave action density  $N(\sigma, \theta)$  per angular frequency  $\sigma$  and direction  $\theta$ , which reads:

$$\frac{DN}{Dt} = \frac{S'}{\sigma} - \frac{S'_b}{\sigma} - \frac{S'_{b,m}}{\sigma} + \frac{S'_{nl}}{\sigma} \quad (1)$$

The wave action density  $N$  is defined as  $N = E'/\sigma$ , where  $E'(\sigma, \theta)$  is the wave energy density and the total wave energy is obtained by integration over frequency and direction:

$$E = \int_0^{2\pi} \int_0^\infty E' d\sigma d\theta \quad (2)$$

The root-mean-square of the orbital velocity at the seabed  $u_{orb}$  and the standard deviation of the water elevation  $\hat{\eta}$  read:

$$u_{orb}^2 = \int_0^{2\pi} \int_0^\infty \frac{\sigma^2}{\sinh^2\{kh\}} \frac{E'}{g\rho} d\sigma d\theta \quad \text{and} \quad (3)$$

$$\frac{1}{2} \hat{\eta}^2 = \frac{E}{g\rho}$$

By definition the significant wave height is  $H_{m0} = 4\hat{\eta}$ . In Eq. (1),  $S'(\sigma, \theta)$  is a source term per wave frequency  $\sigma$  and direction  $\theta$  accounting for wind input,  $S'_b(\sigma, \theta)$  is a sink term accounting for energy dissipation by bed friction, white capping and depth-induced wave braking,  $S'_{b,m}(\sigma, \theta)$  is a sink term accounting for viscous dissipation in the mud layer and  $S'_{nl}(\sigma, \theta)$  accounts for non-linear wave–wave interactions. The first two and fourth terms have been implemented in the standard version of SWAN and are not elaborated here. The third term is modelled further to the two-layer approach by Gade (1958), where we assume that Gade’s approach is applicable per wave direction, and that the individual solutions per wave direction may be added linearly.

Fig. 2 shows the lay-out of the two-layer system and the relevant definitions; the fluid mud layer depicts a bounded internal wave. Free internal wave(s) in the fluid mud layer are irrelevant for the current problem, as these are far too long in relation to the extension of the fluid mud deposits.

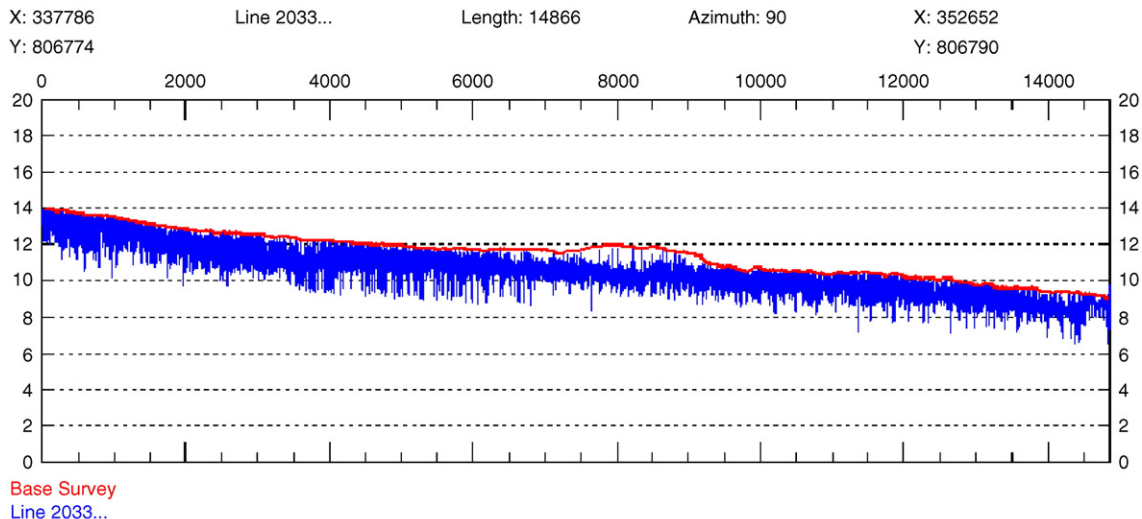


Fig. 6. Filtered acoustic reflections from dual-frequency echo sounding ( $f=210$  and  $33$  kHz) along a cross section in Guyana coastal system perpendicular to the coast.

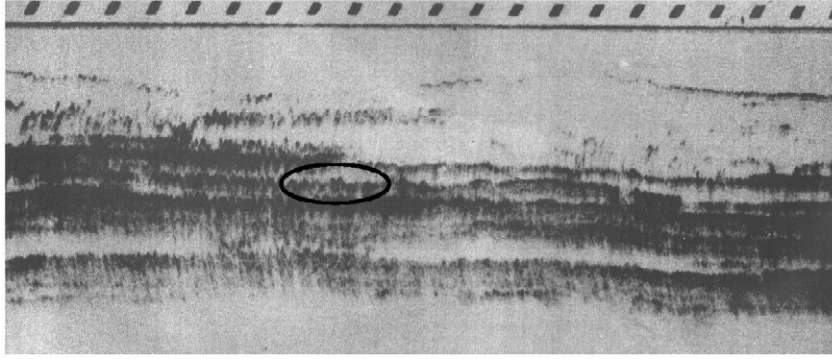


Fig. 7. Acoustic reflections from sub-bottom profiling ( $f \approx 20$  kHz) in Guyana coastal system, Demerara River mouth (Delft Hydraulics Laboratory, 1962) — the vertical scale is estimated to be about 0.5 m.

Gade (1958) limits his analysis to shallow water waves, assumes that the upper layer is non-viscous, and considers that the waves are sinusoidal and small compared to the water depth, so that vertical accelerations can be neglected. Gade’s model was extended by Dalrymple and Liu (1978) by accounting for vertical accelerations (so the model becomes applicable for short waves as well) and a viscous upper layer; by De Wit (1995) accounting for vertical accelerations; by MacPherson (1980) accounting for vertical accelerations and elastic effects in the lower layer; and by Maa and Mehta (1990) accounting for elastic effects in a multi-layered modelled fluid mud layer. Here we follow De Wit (1995), whose approach matches the next phase of our model development best. The two-layer system is then described with the following set of equations for continuity (Eqs. (4) and (6)) and conservation of momentum (Eqs. (5) and (7)) for the upper and lower layers, respectively:

$$\frac{\partial u_1}{\partial x} + \frac{\partial w_1}{\partial z} = 0 \quad (4)$$

$$\frac{\partial u_1}{\partial t} + \frac{1}{\rho_1} \frac{\partial p_1}{\partial x} = 0 \quad (5)$$

$$\frac{\partial w_1}{\partial t} + \frac{1}{\rho_1} \frac{\partial p_1}{\partial x} = -g$$

$$\frac{\partial u_2}{\partial x} + \frac{\partial w_2}{\partial z} = 0 \quad (6)$$

$$\frac{\partial u_2}{\partial t} + \frac{1}{\rho_m} \frac{\partial p_2}{\partial x} = v_m \frac{\partial^2 u_2}{\partial z^2} \quad (7)$$

$$\frac{\partial w_2}{\partial t} + \frac{1}{\rho_2} \frac{\partial p_2}{\partial x} = -g$$

in which  $p_1$  and  $p_2$  are the pressure in the upper and lower layers,  $u_1$  and  $u_2$  are the horizontal flow velocity in the upper and lower layers,  $w_1$  and  $w_2$  are the vertical flow velocity in the upper and lower layers with thickness  $h$  and  $\delta_m$ , respectively, and  $v_m$  is the (constant) fluid mud viscosity. The horizontal and vertical coordinate are given by  $x$  and  $z$  (note that  $x$  is in the direction  $\theta$  of the waves), and  $t$  is time.

This set of equations is solved with the following boundary conditions:

- at free surface ( $z = h + \delta_m$ ):  $p = 0$ ,  $\eta_1 = \hat{\eta}_1 \exp\{i(kx - \sigma t)\}$  and  $w_1 = \partial \eta_1 / \partial t$ ,
- at interface ( $z = \delta_m$ ):  $\partial p / \partial z = 0$ ,  $\partial u_2 / \partial z = 0$  and  $w_1 = w_2 = \partial \eta_2 / \partial t$ , and
- at consolidated bed ( $z = 0$ ):  $u_2 = w_2 = 0$ .

where  $k$  is the complex wave number. Gade solved these equations with the harmonic method, yielding complex wave number and amplitudes of layer thickness and velocity (see also De Wit, 1995). Gade presented results for a uni-directional, mono-chromatic wave field. However, in SWAN a formulation for the energy dissipation  $S'_{b,m}(\sigma, \theta)$  is required. The energy dissipation was obtained by Gade by integrating the work done by the surface waves over the wave period. As said, the relevant wave height was obtained from the harmonic solution of the set of Eqs. (4)–(7). Extending Gade’s analysis<sup>1</sup>, assuming that superposition of the solutions is allowed, the energy dissipation per wave frequency  $\sigma$  and direction  $\theta$  reads:

$$S_{b,m}' = \alpha g h_0 \sigma R \frac{\hat{\eta}_2}{\hat{\eta}_1} \sin\{\phi' - \phi\} E' \quad (8)$$

The complex wave number ( $k = k_r + ik_i$ ) follows from (De Wit, 1995):

$$\left[ \frac{\rho_m - \rho_0}{\rho_m} \frac{gk}{\sigma^2} \left( k \delta_{m,0} - \frac{k}{\lambda_g} \tanh\{\lambda_g \delta_{m,0}\} \right) - 1 \right] \left[ \frac{gk}{\sigma^2} \tanh\{kh_0\} - 1 \right] + \frac{\rho_0}{\rho_m} \left[ k \delta_{m,0} - \frac{k}{\lambda_g} \tanh\{\lambda_g \delta_{m,0}\} \right] \left[ \frac{gk}{\sigma^2} - \tanh\{kh_0\} \right] = 0 \quad (9)$$

where  $\lambda_g = (1-i)\sqrt{\sigma/2v_m}$ . From Eq. (9)  $k_r$ ,  $k_i$ ,  $R (= (k_r^2 + k_i^2)/\sigma^2)$ , and the phase angle between water elevation and flow velocity  $\phi (= 2 \operatorname{atan}\{k_i/k_r\})$  can be computed. The phase angle between surface and internal waves  $\phi'$  follows from:

$$\tan\{\phi'\} = \frac{h_0 g R \sin \phi}{h_0 g R \cos \phi - 1} \quad (10)$$

<sup>1</sup> Note that Gade’s paper contains a (typing) error in the elaboration of the energy loss: Eqs. (II.8), (II.9) and (II.11) should contain a  $\sigma$ .

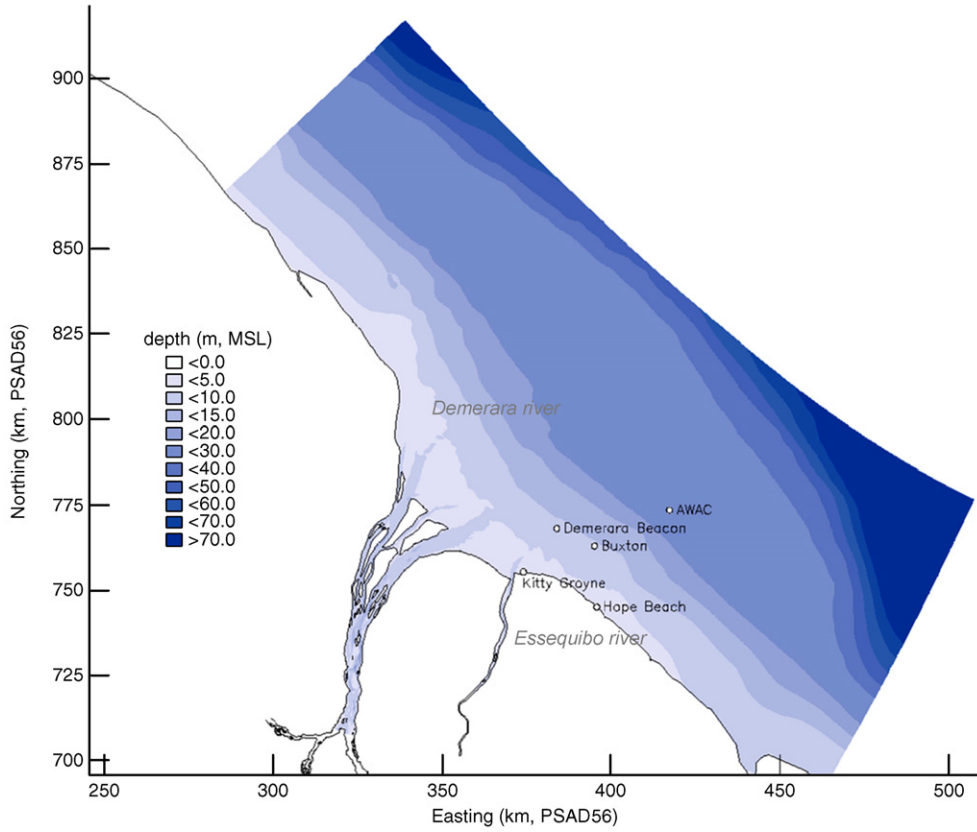


Fig. 8. Depth schematisation of the Guyana wave model.

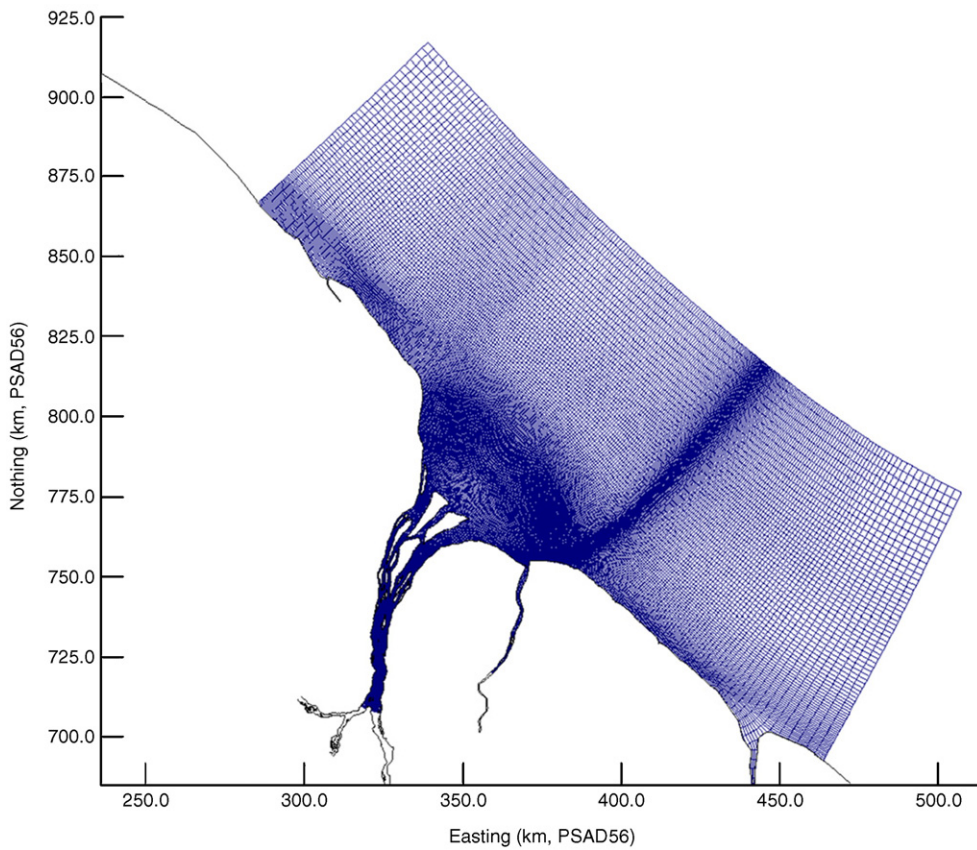


Fig. 9. Computational curvilinear grid of the Guyana wave model.

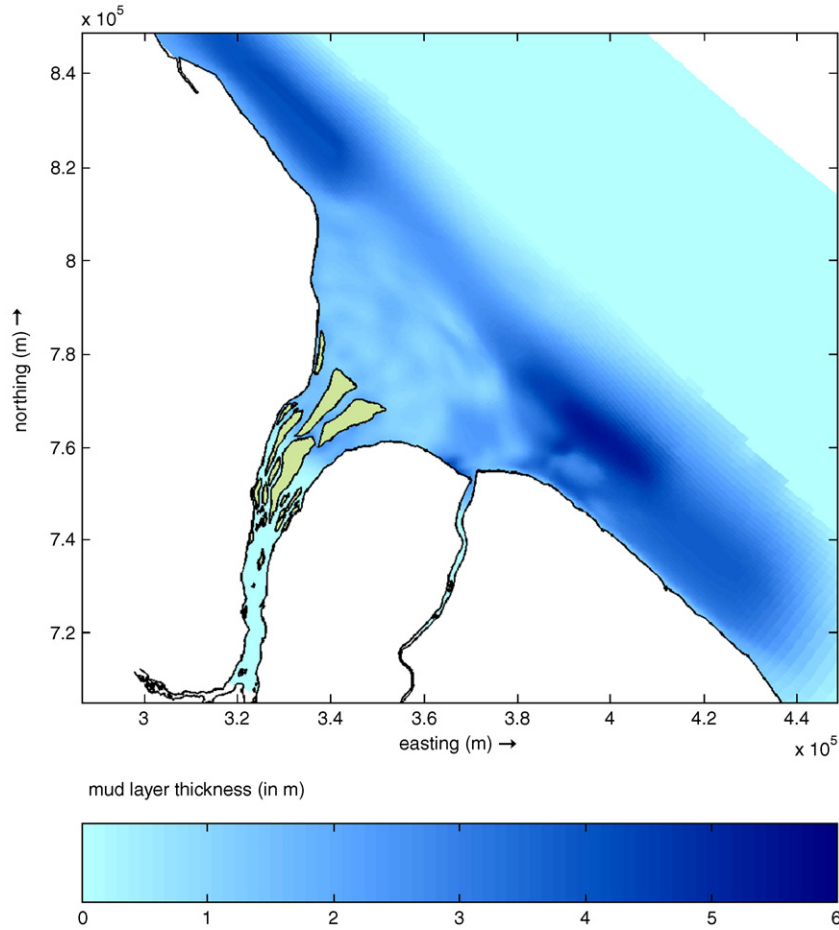


Fig. 10. Mud layer thickness applied in the SWAN mud wave damping model.

Hence,  $S'_{b,m} > 0$ , as  $\phi < |\phi'|$  and  $\phi' < 0$  always holds (e.g. Gade, 1958). The ratio of the amplitudes of surface and internal wave reads:

$$\frac{\hat{\eta}_2}{\hat{\eta}_1} = \sqrt{(1 - gh_0 R \cos\{\phi\})^2 + (gh_0 R \sin\{\phi\})^2} \quad (11)$$

The mud properties  $\delta_m$ ,  $\rho_m$  and  $\nu_m$  follow from measurements or from a fluid mud transport model. Currently, these fluid mud layer properties have to be collected from data or by calibrating the model. In the near future we will incorporate the mud wave damping model with a two-layer fluid mud model and a rheological model. Finally, we have added an extra calibration coefficient  $\alpha$  in Eq. (8) to account for possible non-linear effects allowing a better tuning of SWAN to the observations, if necessary.

Gade (1958) and Dalrymple and Liu (1978) found that the maximum wave attenuation occurs when the thickness of the fluid mud layer amounts to about 1.3 times its viscous boundary layer thickness  $\Delta_m (= \sqrt{\sigma/2\nu_m})$ , which agrees well with Gade's laboratory observations.

### 3. Validation against laboratory experiments

De Wit (1995) carried out wave damping experiments in a 40 m long wave and flow flume, with a width and depth of 0.8 m.

A false floor was mounted to create a 0.2 m deep test section of 8 m length in which a dense mud suspension could be placed. Regular waves were generated with a wave paddle. During the experiments wave height and period were measured, together with vertical profiles of the flow velocity and suspended sediment concentration at a number of places, and the total and pore water pressure at four heights within the dense mud suspension.

Dense mud beds were formed in the test section through consolidation of dilute mud slurries. In this paper we use De Wit's experiment III, test 3, carried out with China clay (the major mineral component of which is kaolinite) to validate the wave damping module in SWAN. A slurry of China clay was prepared in a tank by mixing clay powder with fresh tap water in which 0.5% sodium chloride was dissolved, yielding a sediment

Table 2  
Input parameters and settings for the SWAN mud wave damping model

Parameter	Settings
Thickness of the fluid mud layer $\delta_m$	Spatially varying in computational grid [m]
Density of fluid mud, $\rho_m$	1400 kg/m <sup>3</sup>
Density of water, $\rho_w$	1010 kg/m <sup>3</sup> (at $T = 25$ °C and $S = 20$ ppt)
Viscosity of fluid mud, $\nu_m$	Calibration parameter [m <sup>2</sup> /s], ranging between 0.01 and 0.0001 m <sup>2</sup> /s
Calibration parameter, $\alpha$	1.0 [-]

concentration of about  $275 \text{ kg/m}^3$ . After consolidation for six days, the concentration increased to about  $500 \text{ kg/m}^3$ , i.e. to a density of about  $1300 \text{ kg/m}^3$ . The viscosity of this suspension measured about  $2.7 \cdot 10^{-3} \text{ m}^2/\text{s}$ , i.e. about 300 times larger than that of water. Though, the strength of the mud was not measured, it is estimated to be at about the liquid limit.

Prior to test 3, two other tests were carried out. During test 1, only waves were generated with a height of 22 mm, whereas during test 2 also a net flow was present (velocities of 5, 10 and 15 cm/s) at a wave height of 38 mm. Then the bed was left at rest for another day after which test 3 was carried out with waves of 45 mm, but no current.

Fig. 3 shows the measured variation of wave height at six locations along the flume after equilibrium was attained. It is shown that the wave height at the end of the test section had decreased to about 35 mm, i.e. a reduction of about 20%.

Next, the new SWAN mud wave damping model was used to simulate these measurements. The necessary model parameters were obtained from the measurements by De Wit (1995); De Wit and Kranenburg (1997) and are summarized in Table 1, where  $H_0$  = incoming wave height.

The results of the SWAN simulations are also presented in Fig. 3, showing a favourable agreement between the experimental data and numerical simulation.

## 4. Application to Guyana coast

### 4.1. Observations

Fig. 4 shows an aerial photograph of the breaker zone at Demerara coast of the Guyana coastal system. Towards the west (right-hand part of the photo) white bands of foam, characteristic for wave breaking, are clearly visible. Further to the east, no foam is visible; in fact hardly any waves can be observed.

Unfortunately, no detailed wave data in the Guyana coastal system are available at present from which the wave attenuation over the muddy seabed can be assessed quantitatively. Only some general data have been reported by NEDECO (1972) on decreases in wave heights under average conditions from 1.3 to 0.3 m and under extreme conditions from 4 to 1.2 m. These data are further elaborated in Section 4.2.

However, a good qualitative picture can be obtained from data at a similar site. Fig. 5 depicts the measurements by Wells and Kemp (1986) of wave spectra at three locations in the Surinam coastal waters. The spectra consist of a strong peak at wave periods of  $T_w=9-10 \text{ s}$  representing energy in the swell from the Atlantic Ocean, and a wider band between  $T_w \sim 2$  and  $\sim 5 \text{ s}$ , representing the energy in locally generated waves. The total wave energy has dissipated by about 88% at the middle measuring station (i.e. over a distance of about 9 km) and 96% at the most nearshore station. Note the difference in the vertical scale in the graphs. The conditions at Surinam coast are similar to those at the Guyana coastal, and it is believed that the observations of Fig. 5 are characteristic for the Guyana coastal system as well.

As explained, the strong wave attenuation shown in Figs. 4 and 5 is expected to be caused by viscous dissipation in the liquefied seabed. Unfortunately, up till now we have no direct measurements of liquefaction, and we must rely on physical interpretation of other data. Fig. 6 shows the filtered results of recent dual-frequency echo soundings along a cross section perpendicular to the Guyana coast. The upper signal (210 kHz) represents the top of the soft mud bed, whereas the lower signal (33 kHz) represents some of the structure within the bed. This graph reveals a small pool of fluid mud only, depicted by the gap between the two signals at around  $x=8000 \text{ m}$ . The irregularity of the lower frequency echo signal is typical for layered mud deposits. This is further depicted in Fig. 7, showing reflections from a 20 kHz sub-bottom profiler applied by Delft Hydraulics

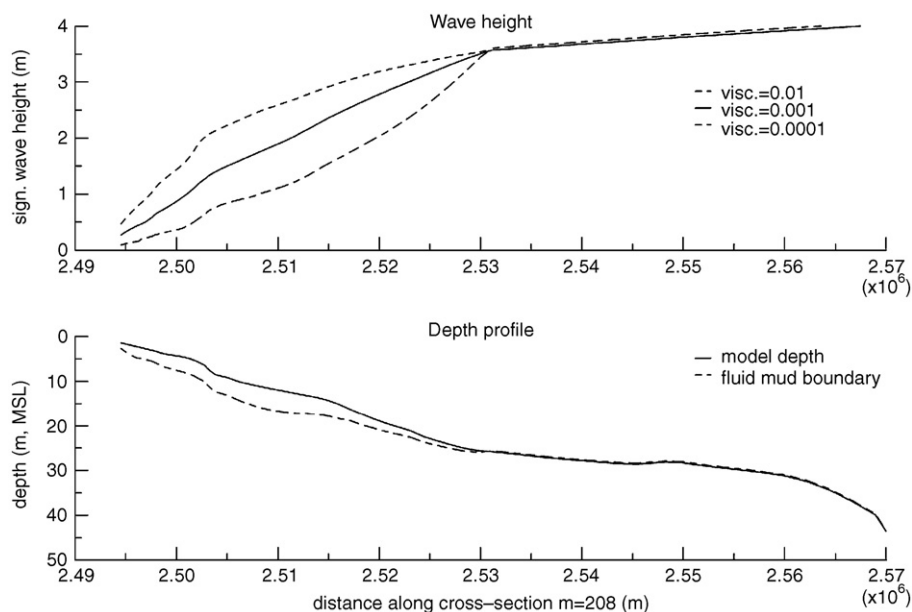


Fig. 11. Cross-shore profiles of significant wave height (top) and depth (bottom) showing the effect of varying viscosity.

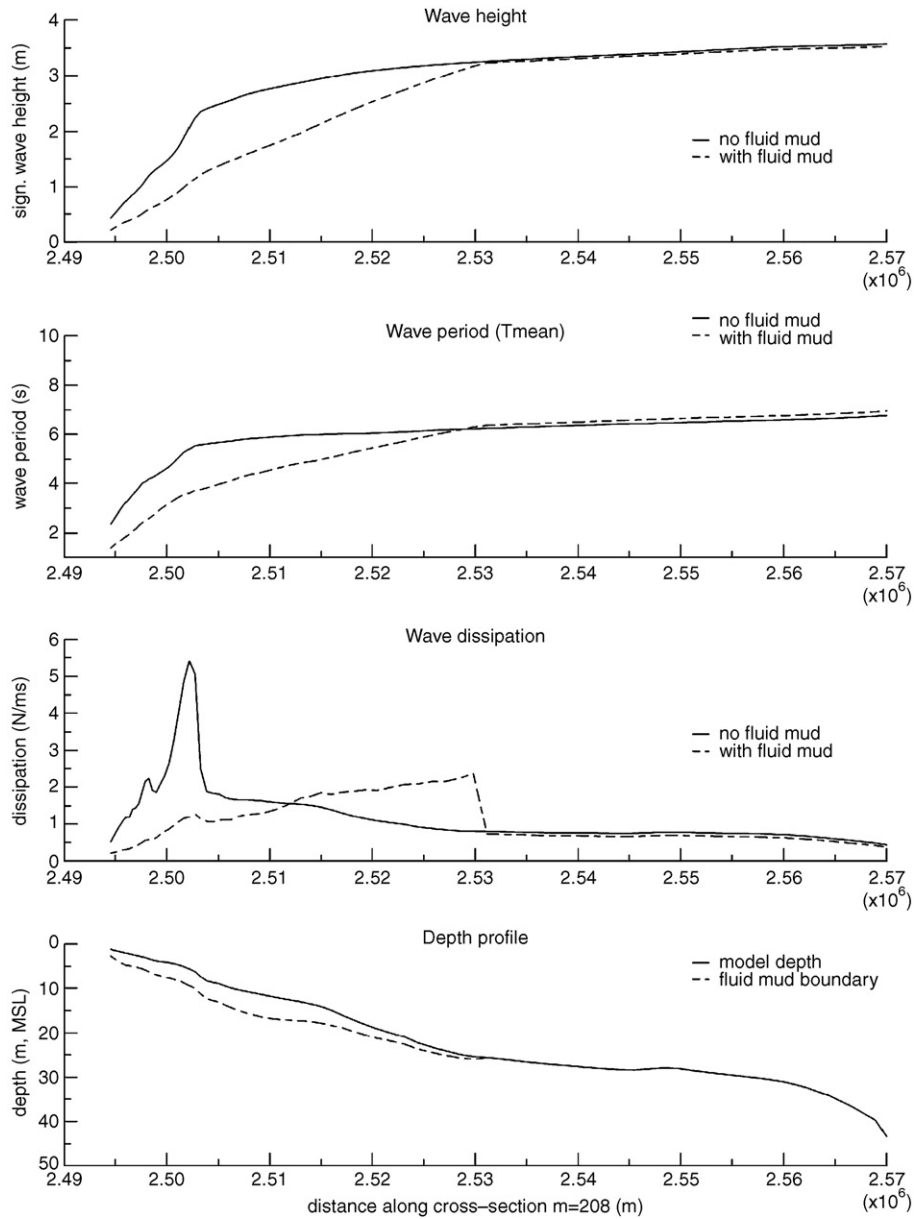


Fig. 12. Computed cross-shore profiles of significant wave height; peak and mean wave period; wave dissipation; and depth profile together with the thickness of the fluid mud layer as schematised in the SWAN mud model ( $\nu_m = 10^{-3} \text{ m}^2/\text{s}$ ).

Laboratory (1962) in the vicinity of Demerara River mouth. The multiple reflections are typical for stratified mud deposits; the thickness of the layers is estimated at about 1–2 dm (the vertical resolution is not known, but can be estimated from the amplitude of the wavy acoustic signal<sup>2</sup>). This layered structure cannot be caused by sedimentation events, as the sedimentation rate in the Guyana coastal system is not driven by episodic events. Hence, this stratification can only be caused by frequent, incomplete liquefaction of the seabed.

From this analysis we deduce, using Figs. 6 and 7, that the thickness of the liquefiable bed in this part of the Guyana coast is about 2 m, and we infer that we can assess the thickness of the

fluid mud layer and its extension from spatial data on the echo soundings (e.g. Section 4.2).

The in-situ density  $\rho_m$ , measured by NEDECO (1972) was found to range from 1300 to 1500  $\text{kg}/\text{m}^3$ . As variations in density cannot be very large, and as the dissipation function is not very sensitive to small variations in density in this range, we take an average value of  $\rho_m = 1400 \text{ kg}/\text{m}^3$ .

Some viscosity measurements have been carried out by NEDECO (1972), as well, with ranges between  $\eta = 0.1\text{--}10 \text{ Pa s}$ . As these data are not very accurate, the viscosity is our main calibration parameter, e.g. Section 4.2.

#### 4.2. Simulations

The modified SWAN model is applied to the wave model covering a large part of the Guyana coastal system, including

<sup>2</sup> These small acoustic waves are marked by an ellipse in Fig. 7. Their amplitude  $a$  follows from  $a = c/f$ , where  $c$  is the speed of sound in the seabed ( $c \approx 1500 \text{ m/s}$ ) and  $f$  is the frequency of the acoustic wave ( $f = 20 \text{ kHz}$ ). Hence,  $a \approx 7.5 \text{ cm}$ .

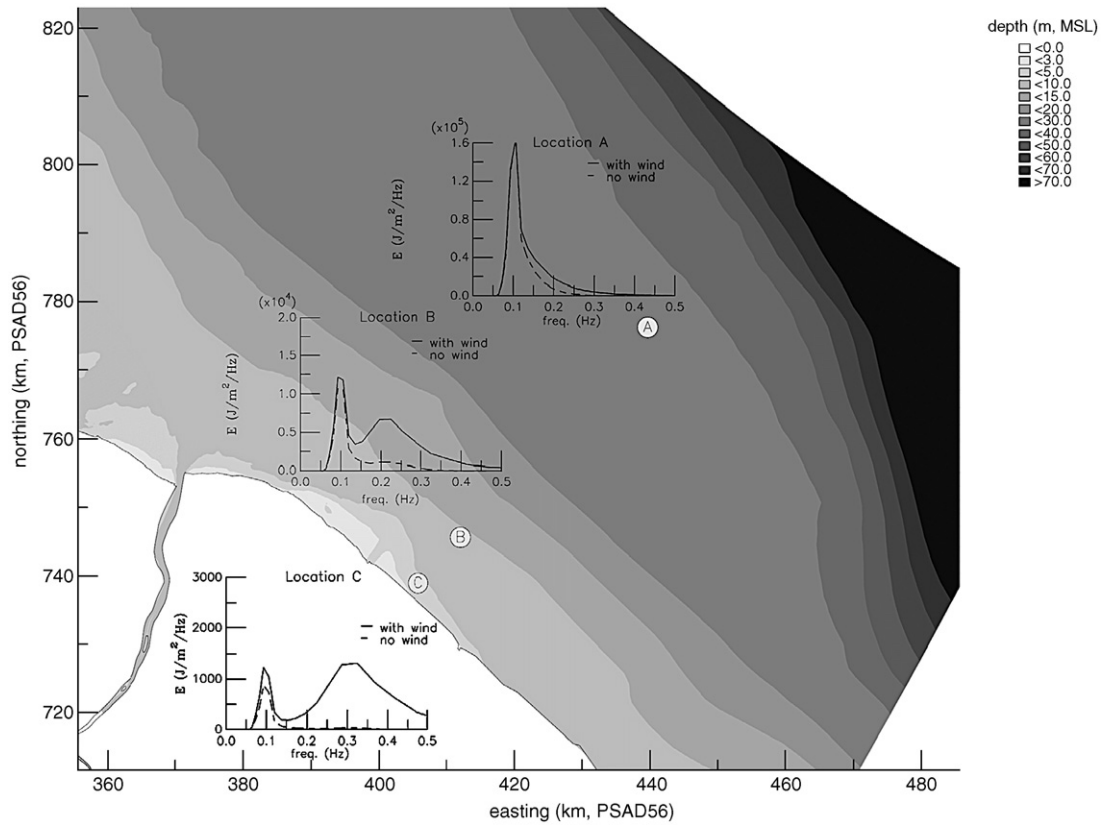


Fig. 13. Computed wave spectrum at three locations in Demerara coastal system with (solid line) and without (dotted line) locally generated waves (note different scales).

the Essequibo estuary (see Fig. 8). The model covers a 250 km wide coastal area and extends about 85 km offshore. The depth at the offshore boundary of the model varies from 135 to 40 m.

The wave model employs a curvilinear grid comprising 263 by 383 points, with approximately 42,000 active points. This computational grid is shown in Fig. 9. The dimensions of the grid cells vary from 2.5 km near the model boundaries to approximately 200 m in the Essequibo estuary, near Georgetown and in the nearshore zone.

Considering the presence of fairly long waves, the width of the energy distribution was taken at  $ms=10$  (a large value of  $ms$  indicates a small directional spreading, typical for long waves; therefore in case of short wind-generated waves  $ms=4$  is generally used) in the wave model. For the wave spectrum a directional resolution of  $10^\circ$  was adopted. The frequency spreading was schematised using 31 discrete frequencies between 0.05 Hz and 1 Hz using a logarithmic scale. For the remaining parameters the default settings of the SWAN model were used.

The SWAN mud wave damping model requires as input the thickness of the (fluid) mud layer. This was defined as the difference between the high-frequency echo reflections and the lowest 10% of the low-frequency reflections (see Section 4.1 and Fig. 6). The resulting spatial varying mud layer thickness varied between 1 m and 5.5 m, as indicated in Fig. 10.

The model was calibrated on the basis of a comparison of average wave heights observed at three nearshore locations, as presented in NEDECO (1972). The observation locations are

indicated in Fig. 8. The objective of the calibration was to optimise the settings of the input variables of the SWAN mud wave damping model. Further calibration of the model on the basis of simultaneous offshore and nearshore measurements was not possible as no simultaneous nearshore wave measurement data were available.

In NEDECO (1972) the average and the maximum wave heights at three nearshore and one offshore locations are presented. Considering the dynamic behaviour of the (mud) bed at the nearshore location, it is very likely that the seabed considerably differs from that at the time the observations were made.

Table 3  
Comparison between historical observations (NEDECO, 1972) and model results with  $\nu_m=0.001 \text{ m}^2/\text{s}$

Location	Observed $H_{m0}$ [m]	Computed $H_{m0}$ [m] with fluid mud	Computed $H_{m0}$ [m] without fluid mud
<i>Average wave conditions</i>			
Offshore	1.3	1.3	1.3
Buxton	0.6	0.6	1.0
Demerara Beacon	0.5	0.6	1.0
Kitty Groyne	0.3	0.1	0.5
<i>Maximum wave conditions</i>			
Offshore	4.0	4.0	4.0
Buxton	2.0	1.6	2.9
Demerara Beacon	1.3	1.5	2.8
Kitty Groyne	1.2	0.4	0.9

Consequently, it is not possible to make a direct comparison between the nearshore observations and model results (based on the present bathymetry). It is therefore not possible to accurately represent these observations. However, we require them to be of the same order of magnitude as an indication as to whether wave energy damping is properly represented by the SWAN mud wave damping model.

As no detailed information was available on the characteristics of the fluid mud itself, the mud parameters had to be assessed from literature or sensitivity analyses. We kept the density of the fluid mud constant, as this is expected not to vary too much. The mud's viscosity was determined by trial-and-error. The selected values are given in Table 2. Computations were carried out with  $\nu_m = 0.01, 0.001$  and  $0.0001 \text{ m}^2/\text{s}$ .

The effect of the varying  $\nu_m$  during an extreme wave condition ( $H_{m0} = 4 \text{ m}$ ,  $T_p = 10 \text{ s}$  accompanied by a NE wind of  $12.5 \text{ m/s}$ ) on the significant wave height is presented in Fig. 11. This figure shows cross-shore profiles (located near Hope Beach, see Fig. 8) of the significant wave height and depth profile as well as the thickness of the fluid mud layer as schematised in the SWAN model. It shows that the mud's viscosity has an important effect on the wave attenuation. This is consistent with the observations by Gade (1958) and Dalrymple and Liu (1978) that the imaginary wave number  $k_i$  peaks at a certain value of the viscous boundary layer thickness, and decreases rapidly at smaller and larger values of the viscosity.

In further analyses  $\nu_m = 10^{-3} \text{ m}^2/\text{s}$  (i.e.  $\eta_m = 1.3 \text{ Pa s}$ ) is used, as this value gave the best results; moreover, this is a typical value for muddy beds at the observed densities. The effect of fluid mud-induced wave damping in the wave computations is shown in Fig. 12 for an extreme wave conditions from the ENE direction. This figure presents cross-shore profiles of the significant wave height ( $H_{m0}$ ); peak and mean wave periods ( $T_p$  and  $T_{m01}$ ); wave dissipation ( $S'_{b,m}$ ); and depth profile and thickness of the fluid mud layer ( $h_0$  and  $\delta_{m,0}$ ) as schematised in the model. Fig. 11 shows that:

1. The mean wave period decreases strongly over the fluid mud layers, with a stronger dissipation of the low-frequency waves;
2. The wave height start to decrease at about 25 m water depth with a relative decrease of up to 50% at about 5 m water depth when taking into account wave damping by fluid mud;
3. Dissipation of wave energy starts at the offshore end of the fluid mud layer and is fairly constant towards the coast. In case wave damping by fluid mud is not included in the wave model, a peak in wave dissipation is found at the coastline, where the waves break due to depth limitation. The latter is not observed in the area of interest of the Guyana coastal system.

The effect of wind-generated waves on the wave climate is illustrated in Fig. 13 by one-dimensional wave spectra at three locations for an extreme wave condition ( $H_{m0} = 4 \text{ m}$ ) from the NE direction. The simulation includes wave damping by fluid mud. Note the growth of wind-generated waves (at a frequency of about 0.2 Hz) towards the coast and the dissipation of the swell (at a frequency of about 0.1 Hz). In this case the peak period shifts from 10 s offshore to 5 s at a nearshore location.

The energy of the  $>0.2 \text{ Hz}$  waves reduces by a factor 3 from A to B, and at their peak by a factor 12. This uneven behaviour in dissipation is due to the effects of bed friction and/or viscous dissipation in the mud layer. The latter effect, however, is by far the larger of the two (e.g. Fig. 12). Note that the shorter waves are only affected directly by the fluid mud at water depths smaller than  $\lambda/2$  (i.e.  $\sim 3 \text{ m}$  for 0.2 Hz waves). However, SWAN accounts for energy transfer from the shorter to the longer waves (and vice versa). Therefore, shorter waves may damp more than expected from the ratio of wavelength and local water depth. The computed wave attenuation towards the coast agrees qualitatively with the measurements by Wells and Kemp (1986), see Fig. 5.

Table 3 presents the comparison between historical nearshore observations described in NEDECO (1972) and the model results with and without the fluid mud-induced wave damping. It is concluded that when including the SWAN mud wave damping model (with the above variable settings), the damping effect of the wave energy is in reasonable agreement with the observations. Wave heights are significantly overestimated in case fluid mud-induced wave damping is not included in the SWAN simulations.

## 5. Discussion

We have modified the two-layer model by Gade (1958) slightly, obtaining a fluid mud-induced wave damping formulation, which was implemented in SWAN. We have ignored, for the time being, the effects elasticity, plasticity and porosity. The new SWAN model has been applied to simulate laboratory experiments and field observations on wave damping in Guyana coastal system. The model results compare favourably with the observations, though detailed field data are not available for an in-depth calibration.

The new SWAN model is a stand-alone programme, and the fluid mud parameters have to be input to the model, comprising the thickness and extension of the mud layer  $\delta_m(x,y,t)$ , and its viscosity  $\nu_m$  and density  $\rho_m$ . The mud's density is not to be expected to vary much, and the mud's viscosity can be established from laboratory experiments. However, establishing  $\delta_m$  forms a fundamental problem, as it is governed by the (initial) wave effects and mud properties, thus determined by strong non-linear feed-back processes. A proper modelling of  $\delta_m$  would require an advanced rheological model, including the effects of plasticity, and possibly of viscosity, and the application of a sediment transport model. Furthermore, at first sight, one may expect that the stress history might be a further complicating factor. However, it can be argued that this is not the case, because stress history is expected to define the maximum thickness of the mud layer that may become subject to liquefaction. This hypothesis will have to be verified, though, using in-situ data.

Though the current approach is promising, further validation is required on the basis of detailed and dedicated surveys, measuring spatial and temporal variations in wave spectra, thickness and extension of fluid mud layers and the mud properties. This is by no means an easy task, as muddy coasts are not very accessible in general. A next step would also be a coupling of the new SWAN

model to a sediment transport model, and the appropriate hydrodynamics, to simulate and predict the long-term evolutions of muddy coasts.

Finally, it is noted that the extension of SWAN proposed in this paper is implemented in the standard version of SWAN, as can be downloaded from the SWAN homepage.

#### List of symbols

$c$	speed of sound
$E$	total wave energy
$E'$	wave energy density
$g$	acceleration of gravity
$H_{m0}$	significant wave height
$h$	water depth
$k$	(complex) wave number
$N$	wave action density
$p$	pressure
$R$	parameter (something like inverse complex wave celerity)
$S'$	wave source term
$S'_b$	“common” wave dissipation term
$S'_{b,m}$	fluid mud-induced wave dissipation term
$S'_{nl}$	source-sink term accounting for non-linear wave–wave interaction
$T_w$	wave period
$T_p$	peak wave period
$T_{m0}$	significant wave period
$t$	time
$u$	longitudinal flow velocity
$u_{orb}$	orbital velocity
$w$	vertical flow velocity
$z$	vertical co-ordinate
$\alpha$	calibration parameter to account for non-linear effects
$\Delta_m$	boundary layer thickness in fluid mud layer
$\delta_m$	thickness fluid mud layer
$\eta$	dynamic viscosity
$\eta_{1,2}$	height of surface, c.q. internal waves
$\hat{\eta}_1$	amplitude surface waves
$\hat{\eta}_2$	amplitude internal waves
$\theta$	wave direction
$\lambda_g$	parameter (something like complex boundary layer thickness)
$\nu_m$	kinematic viscosity mud layer
$\rho_m$	density mud layer
$\rho_w$	density water
$\sigma$	wave frequency
$\phi$	phase angle between elevation and flow
$\phi'$	phase angle between surface and internal wave

#### Acknowledgements

The set-up of a coastal modelling system including the wave mud damping model was carried out under the Institutional Capacity Building Activities (ICBA) project on Guyana’s Sea Defences. The ICBA project is funded by the European Union (8th European Development Fund, no. 8/ACP/GUA/005). We acknowledge Sea Defence Management, and in particular Mr. George Howard and Mr. Mewburn Amsterdam. We thank Mr.

Harry Laboyrie, Mr. Frank Wiersma and Mr. Stephen Pearson from Royal Haskoning (main consultant) for their guidance during the study. Dr. Marcel Zijlema is acknowledged for his help in implementing the “mud module” in SWAN.

Part of this work was carried out under the project “An operational sand–mud model for marine waters” for the U.S. Office of Naval Research, award no. N00173–05–1–G026.

#### References

- Allison, M.A., Lee, M.T., 2004. Sediment exchange between the Amazon mud banks and shore-fringing mangroves in French Guiana. *Marine Geology* 208, 193–203.
- Augustinus, P.G.E.F., 1978. The changing shoreline of Suriname (South America). PhD thesis, University of Utrecht.
- Booij, N., Ris, R.C., Holthuijsen, L.H., 1999. A third-generation wave model for coastal regions, part I: model description and validation. *Journal of Geophysical Research* 104 (C4), 7649–7666.
- Chou, H.-T., 1989. Rheological response of cohesive sediments to water waves. PhD-dissertation. University of California, Berkeley, USA.
- Chou, H.-T., Foda, M.A., Hunt, J.R., 1993. Rheological response of cohesive sediments to oscillatory forcing. In: Mehta, A.J. (Ed.), *Nearshore and Estuarine Cohesive Sediment Transport*. Coastal and Estuarine Studies, vol. 42, pp. 126–147.
- Dalrymple, R.A., Liu, P.L., 1978. Waves over soft mud beds: a two-layer fluid mud model. *Journal of Physical Oceanography* 8, 1121–1131.
- Delft Hydraulics Laboratory, 1962. Demerara coastal investigation. Field survey and basic studies. Report on Siltation of Demerara Bar Channel and Coastal Erosion in British Guyana, vol. 2. The Netherlands.
- De Wit, P.J., 1995. Liquefaction of cohesive sediment by waves. PhD-dissertation. Delft University of Technology, The Netherlands.
- De Wit, P.J., Kranenburg, C., 1997. On the liquefaction and erosion of mud due to waves and current. In: Burt, N., Parker, R., Watts, J. (Eds.), *Cohesive Sediments*. John Wiley & Sons, pp. 331–340.
- Foda, M.A., Tzang, S.-Y., 1994. Resonant waves of silty soil by water waves. *Journal of Geophysical Research* 99 (C10), 20,463–20,475.
- Gade, H.G., 1958. Effects of a non-rigid, impermeable bottom on plane surface waves in shallow water. *Journal of Marine Research* 16 (2), 61–82.
- Golden, S.P., Godwin, J.W., Olal, A.D., 1982. The dependence of the elastic properties of clay dispersions on the mode of interaction between the particles. *Transactions and Journal of the British Ceramic Society* 81 (3), 84–87.
- Jiang, F., 1993. Bottom mud mass transport due to water waves. PhD-thesis. University of Florida, Gainesville, Florida, USA.
- Jiang, L., Zhao, Z., 1989. Viscous damping of solitary waves over fluid-mud beds. *ASCE, Journal of Waterway, Port, Coastal, and Ocean Engineering* 115 (3), 345–362.
- Kurup, 1972. Littoral currents in relation to the mud bank formation along the coast of Kerala. *Mahasagar, Bulletin of the National Institute of Oceanography and Fisheries* 5 (3).
- Lindenberg, J., Van Rijn, L.C., Winterwerp, J.C., 1989. Some experiments on wave-induced liquefaction of soft cohesive soils. *Journal of Coastal Research* 5, 127–138.
- Liu, P.L.-F., 1973. Damping of water waves over porous bed. *ASCE Journal of the Hydraulic Division* 92 (12), 2263–2271.
- Liu, K., Mei, C.C., 1989. Effects of wave-induced friction on a muddy seabed modelled as a Bingham-plastic fluid. *Journal of Coastal Research* 5 (4), 777–789.
- Maa, P.-Y., 1986. Erosion of soft mud beds by waves. PhD-dissertation. University of Florida, Coastal and Oceanographic Engineering Department, Gainesville, Florida, USA, rep. UFL/COEL-TR-059.
- Maa, P.-Y., Mehta, A.J., 1990. Soft mud response to water waves. *ASCE Journal of Waterway, Port, Coastal, and Ocean Engineering* 116 (5), 634–650.
- MacPherson, H., 1980. The attenuation of water wave over a non-rigid bed. *Journal of Fluid Mechanics* 97 (4), 721–742.
- Mei, C.C., Liu, K.F., 1987. A Bingham plastic model for a muddy seabed under long waves. *Journal of Geophysical Research* 94 (C13), 14,581–14,594.

- Mehta, A.J., 1996. Interaction between fluid mud and water waves. In: Singh, V.P., Hager, W.H. (Eds.), *Environmental Hydraulics*. Kluwer Academic Publishers, The Netherlands, pp. 153–187.
- NEDECO, 1972. Report on Sea Defence Studies of British Guyana. NEDECO, The Hague, The Netherlands.
- Rodriguez, H.N., 2000. Mud bottom evolution at open coasts. PhD-dissertation. University of Florida, Coastal and Oceanographic Engineering Department, Florida, USA.
- Rodriguez, H.N., Mehta, A.J., 2001. Modelling of muddy coast response to waves. *Journal of Coastal Research* SI21, 132–148.
- Sheremet, A., Stone, G.W., 2003. Observations of nearshore wave dissipation over muddy sea beds. *Journal of Geophysical Research* 108 (C11) 21–1/21–11.
- Spierenburg, S.E.J., 1987. Seabed response to water waves. PhD-dissertation. Delft University of Technology, The Netherlands.
- Tubman, M.W., Suhayda, J.N., 1976. Wave action and bottom movements in fine sediments. Proceedings of 15th International Conference on Coastal Engineering. ASCE, pp. 1168–1183.
- Verbeek, H., Cornelisse, J.M., 1997. Erosion and liquefaction of natural mud under surface waves. In: Burt, N., Parker, R., Watts, J. (Eds.), *Cohesive Sediments*. John Wiley & Sons, pp. 353–364.
- Wells, J.T., Coleman, J.M., 1981. Physical processes and fine-grained sediment dynamics, coast of Surinam, South America. *Journal of Sedimentary Petrology* 1053–1068.
- Wells, J.T., Kemp, G.P., 1986. Interaction of surface waves and cohesive sediments: field observations and geologic significance. In: Mehta, A.J. (Ed.), *Lecture Notes on Coastal and Estuarine Studies. Estuarine Cohesive Sediment Dynamics*, vol. 14, pp. 43–65.
- Winterwerp, J.C., Van Kesteren, W.G.M., 2004. An introduction to the physical processes of cohesive sediment in the marine environment. Elsevier, *Developments in Sedimentology* vol. 56.
- Yamamoto, T., Takahashi, S., 1985. Wave damping by soil motion. ASCE *Journal of Waterway, Port, Coastal, and Ocean Engineering* 111 (1), 62–77.
- Yamamoto, T., Koning, H.L., Sellmeijer, H., Van Hijum, E., 1978. On the response of a poro-elastic bed to water waves. *Journal of Fluid Mechanics* 87 (1), 193–206.
- Zijlema, M., van der Westhuijsen, A.J., 2005. On convergence behaviour and numerical accuracy in stationary SWAN simulations of nearshore wind wave spectra. *Coastal Engineering* 52, 237–265.